

SPICA and the Chemical Evolution of Galaxies: The Rise of Metals and Dust

J.A. Fernández-Ontiveros^{1,2,3*}, L. Armus⁴, M. Baes⁵, J. Bernard-Salas⁶, A.D. Bolatto⁷, J. Braine⁸, L. Ciesla⁹, I. De Looze¹⁰, E. Egami¹¹, J. Fischer¹², M. Giard^{13,14}, E. González-Alfonso¹⁵, G.L. Granato¹⁶, C. Gruppioni¹⁷, M. Imanishi¹⁸, D. Ishihara¹⁹, H. Kaneda¹⁹, S. Madden⁹, M. Malkan²⁰, H. Matsuhara²¹, M. Matsuura²², T. Nagao²³, F. Najarro²⁴, T. Nakagawa²¹, T. Onaka²⁵, S. Oyabu¹⁹, M. Pereira-Santaella²⁶, I. Pérez Fournon^{1,2}, P. Roelfsema^{27,28}, P. Santini²⁹, L. Silva¹⁶, J.-D.T. Smith³⁰, L. Spinoglio³, F. van der Tak^{27,28}, T. Wada²¹, and R. Wu³¹

Abstract

The physical processes driving the chemical evolution of galaxies in the last ~ 11 Gyr cannot be understood without directly probing the dust-obscured phase of star-forming galaxies and active galactic nuclei. This phase, hidden to optical tracers, represents the bulk of star formation and black hole accretion activity in galaxies at $1 < z < 3$. Spectroscopic observations with a cryogenic infrared (IR) observatory like *SPICA* will be sensitive enough to peer through the dust-obscured regions of galaxies and access the rest-frame mid- to far-IR range in galaxies at high- z . This wavelength range contains a unique suite of spectral lines and dust features that serve as proxies for the abundances of heavy elements and the dust composition, providing tracers with a feeble response to both extinction and temperature. In this work, we investigate how *SPICA* observations could be exploited to understand key aspects in the chemical evolution of galaxies: the assembly of nearby galaxies based on the spatial distribution of heavy element abundances, the global content of metals in galaxies reaching the knee of the luminosity function up to $z \sim 3$, and the dust composition of galaxies at high- z . Possible synergies with facilities available in the late 2020s are also discussed.

Keywords: galaxies: evolution – galaxies: active – galaxies: starburst – infrared: galaxies – techniques: spectroscopic telescopes

Preface

The following set of papers describe in detail the science goals of the future *Space Infrared telescope for Cosmology and Astrophysics (SPICA)*. The *SPICA* satellite will employ a 2.5-m telescope, actively cooled to around 6 K, and a suite of mid- to far-IR spectrometers and photometric cameras, equipped with state of the art detectors. In particular the *SPICA* Far-Infrared Instrument (SAFARI) will be a grating spectrograph with low ($R = 300$) and medium ($R \approx 3\,000$ – $11\,000$) resolution observing modes instantaneously covering the 35–230 μm wavelength range. The *SPICA* Mid-Infrared Instrument (SMI) will have three operating modes: a large field of view ($12' \times 10'$) low-resolution 17–36 μm spectroscopic ($R \sim 50$ – 120) and photometric camera at 34 μm , a medium resolution ($R \approx 2\,000$) grating spectrometer covering wavelengths of 17–36 μm , and a high-resolution echelle module ($R \approx 28\,000$) for the 12–18 μm domain. A large field of view ($80'' \times 80''$), three channel (110, 220 and 350 μm), polarimetric camera will also be part of the instrument complement. These articles will focus on some of the major sci-

entific questions that the *SPICA* mission aims to address, more details about the mission and instruments can be found in [Roelfsema et al. \(2017\)](#).

1 INTRODUCTION

Heavy elements (i.e. elements heavier than He, also known as metals) carry the signature of galaxy evolution. The study of their content and composition in galaxies allows us to look back at the history of the internal recycling of matter: gas accretion feeding star formation episodes and nuclear activity produced by supermassive black holes (SMBH), the enrichment of the gas in the interstellar medium (ISM) or the depletion of heavy elements into dust. The ensemble of the processes involved, known as the “baryon cycle” ([Davé et al. 2012](#)), are invoked to explain fundamental characteristics observed in the present day Universe such as the mass metallicity relation, where the highest metallicities are found in the most massive galaxies ([Tremonti et al. 2004](#); [Gallazzi et al. 2006](#)).

In this scenario, the interstellar and intergalactic media – ISM and IGM, respectively – are progressively enriched with heavy elements after a series of matter cycling. These are

*Email: j.a.fernandez.ontiveros@gmail.com, jafo@iac.es

mixed in the gas-phase of the ISM and IGM, but are also the main components of the solid-phase in the form of dust grains (Draine 2003). Despite their small contribution in terms of mass fraction ($\lesssim 1\%$ of the galaxy mass), heavy elements and dust are fundamental components with a strong influence on the observational properties of galaxies and a main role in the physical and chemical processes that take place in the ISM, e.g. absorption of the optical and UV radiation and re-emission into the infrared (IR), ISM cooling favouring the cloud collapse and subsequent star formation.

Therefore, to understand the physical mechanisms driving the evolution of galaxies, it is essential to probe the products of the baryon cycle over cosmic time. Since the vast majority of star formation and SMBH accretion activity in the universe occurs during a dust embedded phase in the evolution of galaxies (see Madau & Dickinson 2014), the content and composition of metal and dust cannot be accurately derived from tracers in the rest-frame obscured optical range. The use of tracers able to peer into highly obscured environments is mandatory to investigate the content of metals and dust from the peak of star formation activity and SMBH accretion at $z \sim 1-3$ to the Local Universe (e.g. Boyle & Terlevich 1998; Franceschini et al. 1999; Madau & Dickinson 2014; Mancuso et al. 2016). Thus, the answers to fundamental questions in the field of galaxy evolution rely on the contribution of an IR observatory: how are heavy elements and dust produced? how is dust destroyed? Can we describe quantitatively the cycle of matter in galaxies and the physical processes involved? What fundamental physical processes determine the chemical evolution of galaxies?

The present work is focused on the role that a cryogenic IR observatory like the *SPace Infrared telescope for Cosmology and Astrophysics*¹ (*SPICA*; Swinyard et al. 2009, Nakagawa et al. 2014, Sibthorpe et al. 2015, Roelfsema et al. 2017), with its 2.5 m primary mirror actively cooled to around 6 K, would play to understand the chemical evolution of galaxies from $z \sim 3$ till the present time. The *SPICA* observatory has been proposed by a European-Japanese collaboration as the fifth medium-sized class (M5) mission of the European Space Agency (ESA) Cosmic Vision program. In this paper, enclosed in the *SPICA* white paper series on galaxy evolution, we explore the power of *SPICA* in detecting lines and features which can allow robust measurements of the metallicity and dust composition in galaxies. We refer to Spinoglio et al. (2017) for the general overview on *SPICA* studies of galaxy evolution and for the description of the power of IR line diagnostics. The article is organized as follows: in Section 2, we address the key scientific questions that we want to investigate; the main observables, abundance tracers, and dust features available in the mid- to far-IR range are described in Section 3; in Section 4 we discuss the role that *SPICA* would play to address the above science questions; the possible synergies with future facilities available in the

late 2020s are described in Section 5; finally, the main conclusions of this study are summarised in Section 6.

2 THE CHEMICAL EVOLUTION OF GALAXIES

The total content of dust and metals in galaxies is determined by the balance among star formation, the different episodes of gas accretion and ejection (produced by gravity torques and gas inflow motions, and winds and outflows, respectively), and the role of active galactic nuclei (AGN). The influence of these physical processes in the ISM chemistry and its evolution over cosmic time – from the build-up of metals and dust in galaxies till the present time – are still a matter of discussion. However, the past history of galaxy evolution is recorded in the global content and distribution of metals and dust. These are the main products of the matter cycle and show their imprint in the IR spectrum, in the form of continuum emission, spectral lines, and dust spectral features. Moreover, their spatial distribution across the galaxy may also reflect the past activity of the baryon cycle. Thus, a consistent picture describing the role of the different physical mechanisms in the evolution of galaxies should explain, at once, how the global content of metals and dust in galaxies evolves with cosmic time, and how galaxies were assembled.

In this context, we identify three main questions in the field of chemical evolution whose answers are key to understand how galaxies have evolved in the last ~ 11 Gyr: *i*) how are metals distributed within galaxies? *ii*) how did the global content of metals in galaxies evolve with cosmic time? and *iii*) how did metals locked into dust grains evolve from high- z till the present time?

2.1 The Assembly of Galaxies

Current models of galaxy formation predict that galaxy discs form through accretion of matter in an inside-out growth, with a combination of inflow and outflow events regulating the process of metal enrichment (Fu et al. 2009; Davé et al. 2012; Anglés-Alcázar et al. 2014). The accreted gas reaches higher densities in the interior of the galaxy, leading to higher star formation rates and a faster reprocessing of gas, which results in higher metallicities in the bulge and in the inner part of discs. This is followed by a decreasing metallicity towards outer regions, populated by younger stars formed from poorly enriched material (e.g. González Delgado et al. 2015). While outflow activity is potentially capable of transferring the high abundance of metals to the halo or even the IGM (Oppenheimer & Davé 2006), and subsequent inflows can further recycle them, observations have to be performed to ascertain the history of chemical evolution and the way in which outflows and inflows have shaped it (see also González-Alfonso et al. 2017). Since the spatial distribution contain the imprint of gas inflow and outflow episodes throughout the lifetime of these galaxies, tracing the spatial gradients of heavy element abundances in present

¹<http://www.spica-mission.org>

day galaxies provides a unique insight into their evolutionary history.

2.2 The Evolution of Metallicity in Galaxies

The ISM of massive galaxies shows a higher content of heavy elements when compared to less massive ones, as was discovered early by [Lequeux et al. \(1979\)](#). Later [Mannucci et al. \(2010\)](#) and [Lara-López et al. \(2010\)](#) incorporated an additional dependency on the SFR required to describe the evolution of galaxies up to $z \sim 3.7$. Thus, the impact of the baryon cycle determines the relation among fundamental properties of galaxies such as the gas metallicity, the stellar mass, and the SFR. This is illustrated in [Figure 1](#), where the mass-metallicity relation is obtained for galaxies in different bins of SFR ([Andrews & Martini 2013](#)). The metallicities in [Fig. 1](#) are based on the direct method, i.e. using the weak auroral lines to determine the gas temperature, the latter is one of the main uncertainties of the strong-line method based on the calibration of bright emission lines sensitive to the metallicity (e.g. [Tremonti et al. 2004](#), see [Section 3](#) for further details). Thereafter [Bothwell et al. \(2013\)](#) interpreted the dependence on the SFR as a by-product of the molecular gas content, via the Schmidt-Kennicutt relation ([Schmidt 1959](#); [Kennicutt 1998](#)). In this scenario, the chemical enrichment is driven by the increase of the specific SFR due to the larger disc gas fractions in galaxies at high- z ([Bothwell et al. 2016a,b](#)), and can be triggered by the accretion of pristine gas from the cosmic web and/or mergers with metal-poor companions ([Hunt et al. 2016a,b](#)). On the other hand, outflows of enriched material dominate at low-redshift, explaining the correlation with the stellar mass (e.g. [Peeples & Shankar 2011](#); [Davé et al. 2011](#); [Somerville & Davé 2015](#)).

In the present-day picture, the relation between galaxy mass and gas metallicity is a by-product of the internal cycle of matter in galaxies during their evolution with cosmic time ([Davé et al. 2012](#)), and it is due to several reasons: *i*) starburst wind outflows in low-mass galaxies eject the metal-enriched material to the halo and the IGM due to the shallow gravitational potential well, resulting in a less efficient enrichment compared to massive galaxies ([Tremonti et al. 2004](#)); *ii*) the “galaxy downsizing” scenario, i.e. low-metallicity galaxies in the Local Universe are associated with a high specific SFR and are found in low-mass systems, which are still in an early evolutionary stage because they have converted only a small fraction of their gas mass into stars (e.g. [Brooks et al. 2007](#)); *iii*) dependence of the shape of the initial mass function (IMF) with the galaxy mass ([Köppen et al. 2007](#)); and *iv*) infall of metal-poor gas from the halo and/or the IGM ([Finlator & Davé 2008](#); [Brooks et al. 2009](#)).

If the same physical processes are in place in the Local Universe and at high- z , then the chemical evolution of galaxies should be governed by a reduced number of fundamental properties. Diverse models of galaxy formation and evolution predict manifold evolutionary patterns of the mass-metallicity relation as a function of redshift. These patterns

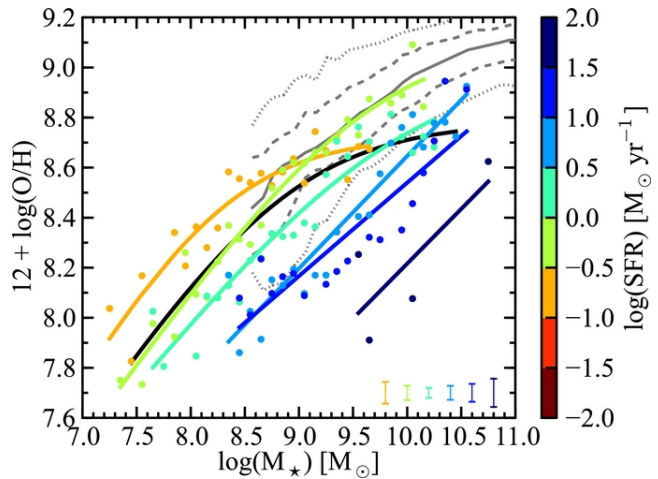


Figure 1. The mass-metallicity relation determined from direct abundance measurements based on optical fine-structure lines for $\sim 200\,000$ star-forming galaxies selected from the Sloan Digital Sky Survey ($0.027 < z < 0.25$), grouped in different bins of SFR. The colour coded circles correspond to stacks of galaxies for each bin in SFR (mean error is indicated in the lower right). The coloured solid lines show asymptotic logarithmic fits to this relation for each bin in SFR, and the black-solid line in the centre of the figure shows the global fit. These are compared with the mass-metallicity relation from [Tremonti et al. \(2004\)](#), based on the strong-line method (the solid, dashed, and dotted grey lines correspond to the median, 68%, and 95% contour of the relation, respectively). Figure adapted from [Andrews & Martini \(2013\)](#).

lead to different properties in the modelled galaxies such as the slope of the mass-metallicity relation and its scaling with redshift, scatter around the mass-metallicity relation due to fluctuations in the baryon cycle activity, and the mass fraction of atomic and molecular gas (e.g. [Davé et al. 2017](#)). So far, most of the models reproduce the growth of the stellar mass in galaxies over cosmic time, but the global content of heavy elements and the gas fraction are largely unconstrained. Therefore, observational data of galaxies from high- z to the Local Universe are required to test these properties, discriminate among the different cosmological simulations, and understand the physical processes driving the chemical evolution in galaxies.

2.3 The Build-Up of Cosmic Dust

Heavy elements produced in the baryon cycle are partially locked into dust grains, and constitute the solid-phase of the ISM ([Draine 2003](#); [Peimbert & Peimbert 2010](#)). The dust has a strong influence on the observational properties of galaxies, with a main role in the heating and cooling processes ([Spitzer 1948](#); [Borkowski & Harrington 1991](#); [van Hoof et al. 2001](#)), and as catalyst of chemical processes in the ISM (e.g. the formation of H_2 driving the molecular chemistry). Dust grains absorb the UV light and re-radiate it in the IR, shielding the dense gas and by these means triggering the formation of molecular clouds where new stars

are born. The grain surfaces and the polycyclic aromatic hydrocarbons (PAHs) participate in a large number of chemical reaction networks in different phases of the ISM (Bakes & Tielens 1998), and also provide photoelectric heating of gas in photo-dissociation regions (Draine 2011; Bakes & Tielens 1994). Moreover, dust cooling is able to alter the shape of the IMF by favouring the cloud fragmentation, thus inhibiting the formation of massive stars and fostering the creation of low-mass stars (Omukai et al. 2005). On the other hand, dust grains suffer from processing and destruction due to intense radiation fields, sputtering (impacts with gas ions), shattering (grain-grain collisions), shocks due to SNe explosions, astration into newly formed stars, and photo-processing by cosmic rays and UV/X-ray fields in the vicinity of AGN.

Little is known on the dust chemistry and its evolution over cosmic time. Even in the Milky Way and its neighbourhood, fundamental aspects in the astrochemistry of dust are not well understood: the dust composition in star forming regions (Peimbert & Peimbert 2010), the ISM (e.g. Nieva & Przybilla 2012), and planetary nebulae (PNe; Clegg & Harrington 1989; Bernard-Salas et al. 2009b); the depletion of elements onto dust grains (e.g. Delgado Inglada et al. 2009; Simón-Díaz & Stasińska 2011); the dust-to-gas ratios, grain size distribution, and dust destruction (Mallik & Peimbert 1988; Stasińska & Szczerba 1999; van Hoof et al. 2013; Asano et al. 2013b); the physical mechanisms involved in the dust-phase catalysis within the ISM and subsequent enrichment of the gas-phase (Dulieu et al. 2013). Nevertheless, the dust composition and its properties are critical ingredients to describe the evolution of galaxies (Rémy-Ruyer et al. 2014), while the uncertainties mentioned above escalate significantly for studies of galaxies at high- z (e.g. Popping et al. 2017). Currently, models describing the chemical evolution in galaxies (e.g. Asano et al. 2013a) rely on dust studies in local metal-poor dwarfs (e.g. Rémy-Ruyer et al. 2015), which are usually adopted as a benchmark case for the ISM in galaxies at high- z . However, there is firm observational evidence suggesting that the dust properties are not universal, e.g. chemical composition, gas-to-dust and dust-to-metal ratios, and grain size distribution (see Zhukovska et al. 2016, and references therein). The characteristics of dust in the early Universe may be quite different from those seen in local metal-poor dwarfs, thus probing the dust properties in galaxies at high- z is the only way to constrain the solid phase of the ISM in chemical evolution models.

3 METALLICITY TRACERS IN THE INFRARED

An accurate description of the chemical evolution in galaxies requires reliable tracers to quantify the abundances of the different chemical species in the ISM. Specifically, it is essential to use appropriate tracers able to peer into the dust-embedded phase in the evolution of galaxies, which represents the bulk of the star formation and black hole accretion activity (Madau & Dickinson 2014; Mancuso et al. 2016).

So far, the vast majority of studies probing the abundances of heavy elements and their evolution with redshift rely on the determination of oxygen abundances using optical line diagnostics. Among them one can distinguish two main types of diagnostics, those based on the determination of the electron temperature using the weak auroral lines (the direct method; e.g. Izotov et al. 1994, 1997; Izotov & Thuan 1999; Kennicutt et al. 2003; Hägele et al. 2008), and those based on the calibration of bright emission-line ratios sensitive to the gas metallicity (Pagel et al. 1979; McGaugh 1991; Pilyugin 2001a; Pilyugin & Thuan 2005; Dors & Copetti 2005). The main limitations that affect optical-based tracers are: *i*) dust obscuration, which restricts the abundance measurements to the unobscured regions in galaxies; *ii*) poor determination of the electron temperature, which is based on temperature-sensitive auroral lines (e.g. [O III] λ 4363, [N II] λ 5755), typically faint and difficult to detect (Bresolin et al. 2005; Moustakas et al. 2010); *iii*) systematic discrepancies in the calibration of strong-line abundance diagnostics, based on the brightest collisionally-excited lines such as [O III] λ 4959, 5007, [N II] λ 6548, 6584, [S II] λ 6716, 6731, H α , and H β . Although these calibrations provide reliable abundances in relative terms, they show large systematic discrepancies (up to ~ 0.7 dex) in the absolute oxygen abundances derived among the various empirical and theoretical calibrations for the line ratios (see Kewley & Ellison 2008, and references therein). This is especially the case at high- z (Kewley et al. 2006), where physical conditions in the ISM can be significantly different than those in nearby galaxies. Furthermore, they also show a different turnover in the mass-metallicity relation when compared to direct metallicity determinations (see black- and grey-solid lines in Fig. 1; Andrews & Martini 2013); *iv*) temperature fluctuations across the nebula – e.g. produced by variations in the chemical abundances or densities – can lead to an error in the abundance estimates based on optical lines of a factor ~ 4 (Dors et al. 2013). Moreover, except for the case of oxygen which shows strong emission lines for its main chemical species in the optical (e.g. [O I] λ 6300, 6364, [O II] λ 3726, 3729, [O III] λ 4959, 5007), the rest of element abundances have to rely on uncertain ionisation correction factors to account for the unobserved stages of ionisation. Commonly adopted metallicity calibrations (i.e. indirect methods), based on the ratios of strong emission lines in the optical and UV range, are: the index $R_{23} \equiv ([\text{O II}]\lambda 3727 + [\text{O III}]\lambda 4959, 5007)/\text{H}\beta$ (Pilyugin 2001b; Pilyugin & Thuan 2005); the index $N_2 \equiv [\text{N II}]\lambda 6584/\text{H}\alpha$ (Pettini & Pagel 2004); the index $\text{O}_3\text{N}_2 \equiv ([\text{O III}]\lambda 5007/\text{H}\beta)/([\text{N II}]\lambda 6584/\text{H}\alpha)$ (Pettini & Pagel 2004); a combination of [N II] λ 6584, H α , and [S II] λ 6717, 6731 (Dopita et al. 2016); in the UV, the index $C_{43} = \log((\text{C IV } \lambda 1549 + \text{C III } \lambda 1909)/\text{He II } \lambda 1640)$ for AGN (Dors et al. 2014); and a combination of the indices $C_3\text{O}_3 = \log((\text{C IV } \lambda 1549 + \text{C III } \lambda 1909)/[\text{O III}]\lambda 1664)$, $C_{34} = \log((\text{C IV } \lambda 1549 + \text{C III } \lambda 1909)/\text{H I})$ (where H I corresponds to a hydrogen recombination line, e.g. H β), and $C_3\text{C}_4 =$

$\log(C\text{ III}] \lambda 1909 / C\text{ IV} \lambda 1549)$ for star forming regions (Pérez-Montero & Amorín 2017).

3.1 Why IR tracers?

The use of robust metallicity tracers almost independent of the dust extinction, radiation field, and of the gas density are crucial to study the chemical evolution of galaxies. For instance, the metallicity inferred from the dust content of high- z sub-millimetre galaxies (SMG), determined with *Herschel* far-IR photometry, is more than an order of magnitude higher when compared to gas metallicity measurements based on optical nebular lines (Santini et al. 2010). This discrepancy is most probably caused by dust obscuration. Since SMG are compact and dust-rich, most of the ISM is optically thick at visual wavelengths. Thus, the optical nebular lines only probe the outer parts of the star-forming regions, which are probably hardly enriched with heavy elements.

Abundance determinations based on mid- and far-IR lines offer two great advantages when compared to those derived from UV and optical lines: *i)* IR lines are almost free from dust extinction; and *ii)* they have a small dependency on the electron temperature (e.g. Bernard-Salas et al. 2001). The latter could be the origin of a known discrepancy between optical and IR tracers, where IR-based abundances tend to be higher when compared to those obtained using optical tracers (see Vermeij & van der Hulst 2002; Dors et al. 2013). A comprehensive explanation of this discordance is still lacking, and therefore there is not a consensus in the field on what tracer (optical or IR) is more reliable. However, a possible explanation is given in Dors et al. (2013): temperature variations within the nebula that not resolved spatially in the spectra – e.g. produced by spatial variations in the chemical abundances – can lead to a systematic underestimation of the abundances derived from optical lines using the direct method by a factor $\lesssim 4$ (0.6 dex). For instance, this is the case of integrated spectra in galaxies. If confirmed, this result implies that tracers based on IR lines can be much more accurate, since their dependency on the electron temperature is feeble. Unfortunately, there are few galaxies where both methods can be applied and compared. Sensitive IR observations with the *SPICA* observatory for a sample of galaxies with available optical metallicity estimates would be essential to shed light on this issue and develop new and reliable abundance tracers.

In the Local Universe, *SPICA* would have access to several ionic fine-structure lines in the rest-frame mid- and far-IR spectra of galaxies. Thus, abundance diagnostics for heavy elements will be mainly based on ratios of these lines, which can be calibrated using photoionisation models such as CLOUDY (Ferland et al. 2017) and MAPPINGS². The weak dependence with density can be easily constrained using density-sensitive ratios such as $[N\text{ II}]_{122\mu\text{m}} / [N\text{ II}]_{205\mu\text{m}}$, $[O\text{ III}]_{52\mu\text{m}} /$

$[O\text{ III}]_{88\mu\text{m}}$, $[S\text{ III}]_{18.7\mu\text{m}} / [S\text{ III}]_{33.5\mu\text{m}}$, $[Ne\text{ III}]_{15.6\mu\text{m}} / [Ne\text{ III}]_{36.0\mu\text{m}}$, and $[Ne\text{ V}]_{14.3\mu\text{m}} / [Ne\text{ V}]_{24.3\mu\text{m}}$ (Croxall et al. 2013). Furthermore, the hardness of the radiation field can also be constrained using the line ratios of $[N\text{ III}]_{57\mu\text{m}} / [N\text{ II}]_{122,205\mu\text{m}}$, $[Ne\text{ III}]_{15.6\mu\text{m}} / [Ne\text{ II}]_{12.8\mu\text{m}}$, and $[O\text{ IV}]_{25.9\mu\text{m}} / [O\text{ III}]_{52,88\mu\text{m}}$. On the other hand, the effects on the fine-structure lines produced by the combination of high far-infrared optical depths and high ionisation parameters found in luminous and ultraluminous IR galaxies (LIRGs and ULIRGs, respectively; Graciá-Carpio et al. 2011, Fischer et al. 2014, González-Alfonso et al. 2015) can also be calibrated with photoionisation models (e.g. Abel et al. 2009, Graciá-Carpio et al. 2011, Fischer et al. 2014).

Besides the gas-phase abundances, a sensitive telescope in the mid- to far-IR range would be able to probe the composition of dust in galaxies at high- z through several solid-state features in the spectrum, such as forsterite (Mg_2SiO_4 ; 23, 33, 69 μm), water ice at 44 and 62 μm , MgS and FeS at ~ 30 μm , FeO and SiO_2 at around 21 μm , iron-bearing crystalline silicates at ~ 55 μm (Koike et al. 2003), fullerenes (C_{60} and C_{70}), and PAHs (see the companion paper by Kaneda et al. 2017 in this issue).

So far, the use of IR tracers based on mid- to far-IR spectroscopic observations with *Spitzer* and *Herschel* to study the chemical evolution of galaxies was restricted only to very luminous sources, due to sensitivity issues (e.g. Ruiz et al. 2013; Brisbin et al. 2015). Future facilities planned for the next decade will not cover this key spectral range. Therefore their study of the chemical evolution in galaxies will be limited to unobscured regions in galaxies, and will rely on tracers with a strong dependency on the gas temperature (see Section 5).

The unique sensitivity of an IR observatory with the characteristics of *SPICA* would enable the study of key processes in the baryon cycle that are hidden to optical wavelengths. A description of the *SPICA* spectrometers, SMI and SAFARI, is given in Roelfsema et al. (2017). Fig. 2 shows the predicted spectra for starburst galaxies and AGN out to $z = 4$, assuming the spectral characteristics of a local starburst galaxy, and an AGN. The simulated spectra in this figure are based on the *ISO/SWS* + *LWS* and *Spitzer/IRS* observations of the starburst galaxy M82 and the Seyfert 2 galaxy NGC 1068. These galaxies were selected due to the availability of high S/N *ISO-SWS* and *-LWS* spectra which, combined with the high-spectral resolution *Spitzer/IRS* observations, allowed us to build spectral templates with a wide coverage in wavelength from 10 to 250 μm , similar to the rest-frame range that would be accessible to *SPICA*. The spectra of both galaxies were scaled to a luminosity of $2 \times 10^{12} L_{\odot}$, and located at $z = 1, 2, 3$, and 4 (from top to bottom). The different observational modes of SMI and SAFARI would be sensitive enough to provide access to a unique suite of IR lines in the mid- to far-IR rest-frame spectra of starburst galaxies and AGN at the knee of the luminosity function up to $z \sim 3$.

In the following sections we will focus on the observational strategies that *SPICA* could implement to determine heavy

²<https://mappings.anu.edu.au/code>

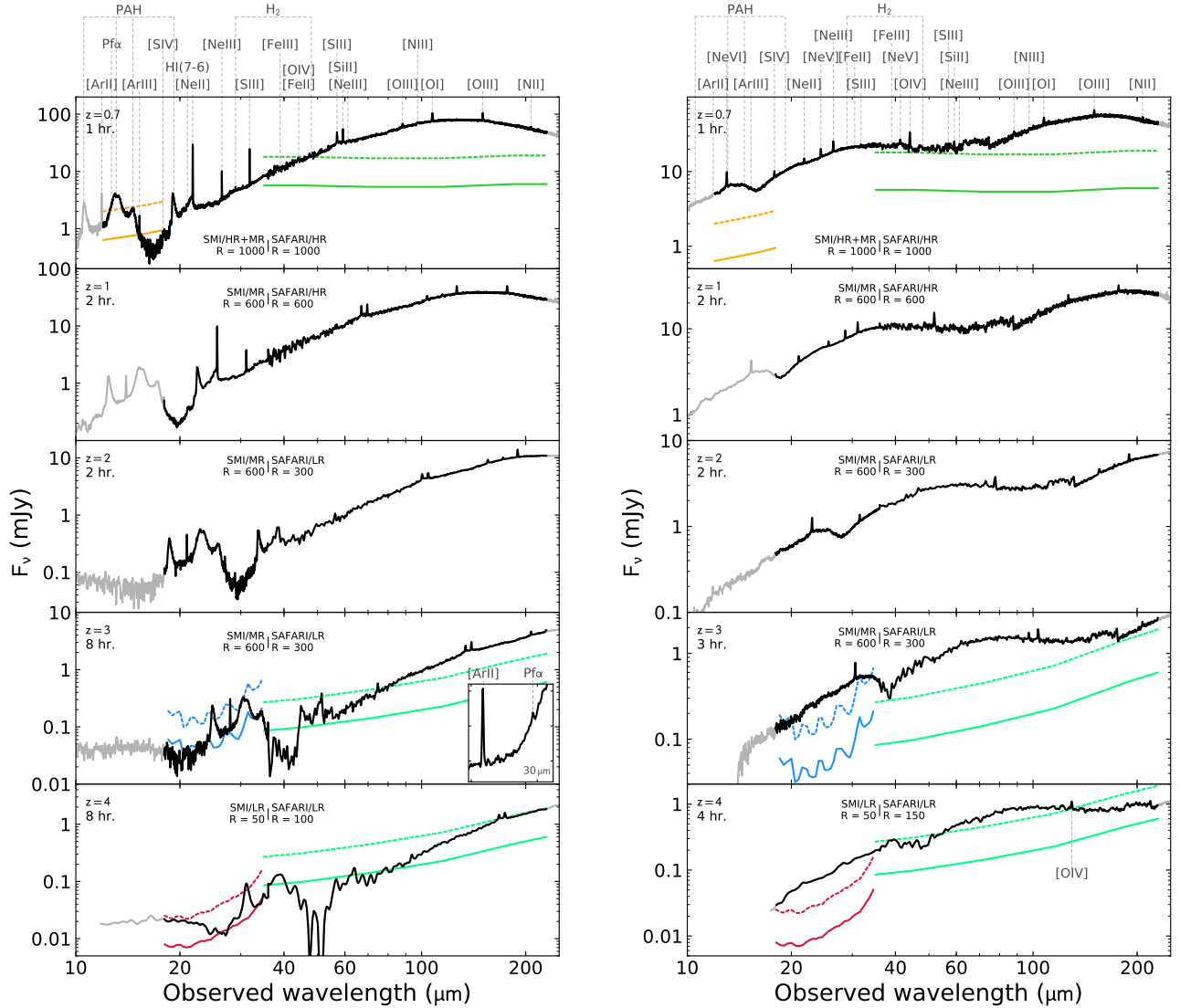


Figure 2. Simulated spectra for a starburst galaxy (left) and an AGN (right) with a luminosity of $2 \times 10^{12} L_{\odot}$ in the $z = 1-4$ range, assuming the spectral characteristics of M82 and NGC 1068, respectively, observed with *ISO/SWS + LWS* and *Spitzer/IRS*. The spectra are simulated at $z = 1, 2, 3$ and 4 , from top to bottom. In each case, white noise was added to the spectra with an amplitude of $1\sigma/\sqrt{t}$, t being the exposure time assumed (indicated in the upper-left corner of each panel). Finally, the SMI and SAFARI spectral ranges were binned to the spectral resolution values indicated in each frame. The *SPICA* 5σ sensitivities for SMI (MR mode in blue, $R \sim 1500$; LR mode in red, $R \sim 100$) and SAFARI (in green, HR mode in the upper panels at $z = 0.7$; LR mode, $R \sim 300$, in the lower panels) are indicated for integration times of 1 hour (dotted lines) and 10 hours (solid lines). The Pfund- α would be detected in the $1.5 < z \lesssim 3$ range (see inset on the left panel at $z = 3$).

element abundances of galaxies from high- z to the Local Universe. First, we will describe the direct abundance determinations in Section 3.2, followed by the indirect methods in Sections 3.3 and 3.4. The main diagnostics are summarised in Table 1.

3.2 Direct Abundance Determinations

A direct determination for the abundances of the main ionic stages of several heavy elements could be obtained using ratios of IR fine-structure lines to hydrogen recombination lines. In the case of *SPICA*, this would be possible using Pfund- α – at $7.46 \mu\text{m}$ in the rest frame – or Humphreys- α – H 1(7-6) or $\text{Hu}\alpha$ at $12.37 \mu\text{m}$. At $1.5 < z \lesssim 3$, the medium-resolution mode (MR, $R \sim 1500$) of SMI would be

Table 1 Direct (upper rows) and indirect (lower rows) metallicity tracers based on the mid- to far-IR lines that could be exploited by *SPICA*. In the table, “[X]” refers to any of the fine-structure lines found in the range accessible to *SPICA* (e.g. [S III]_{18.7μm}, [Ar II]_{6.99μm}, [Ne II]_{12.8μm}) whose corresponding ionic stage abundance can be determined from the flux ratio of the [X] line to any of the hydrogen recombination lines. The *Huα* line is relatively weak and thus is expected to be detected only in nearby galaxies ($z \sim 0$).

Type	Redshift range	Tracer
Direct	Local	$\frac{[X]}{H\alpha}$
	1.5–3	$\frac{[X]}{Pfund\alpha}$
Indirect	0–1.6	$\frac{2.2 \times [OIII]_{88\mu m} + [OIII]_{52\mu m}}{[NIII]_{57\mu m}}$
	0–3.0	$\frac{[OIII]_{52\mu m}}{[NIII]_{57\mu m}}$
	0.15–3	$\frac{[NeIII]_{12.8\mu m} + [NeIII]_{15.6\mu m}}{[SII]_{18.7\mu m} + [SIV]_{10.5\mu m}}$

able to cover simultaneously *Pfund-α* and the argon lines [Ar II]_{6.99μm} and [Ar III]_{8.99μm}. For instance, *Pfund-α* could be detected by SMI/MR in a starburst galaxy with similar spectral characteristics to M82, scaled to $2 \times 10^{12} L_{\odot}$, as shown by the inset in Fig. 2 (left panel, at $z = 3$). Then, the gas metallicity could be estimated from the ratio of argon to hydrogen lines, since argon does not suffer from depletion (Verma et al. 2003). Since the ionisation potentials of Ar⁰ and Ar²⁺ are 15.8 eV (> 13.6 eV) and 40.7 eV (< 54.4 eV), respectively, the presence of Ar⁰ and Ar³⁺ could be expected. In the case of neutral argon, observations of star forming regions do not show a significant contribution from this species, suggesting that most of the argon in the nebula is ionised (e.g. Leboutteiller et al. 2004, 2006). This could be explained by a high photoionisation cross section in the neutral argon (Sofia & Jenkins 1998). On the other hand, Ar²⁺ has a relatively low photoionisation cross-section for energies below 70 eV (Verner et al. 1996), and thus Ar³⁺ has a minor contribution for most H II regions ($\lesssim 3\%$, e.g. Peimbert 2003; Tsamis et al. 2003; García-Rojas et al. 2006; Leboutteiller et al. 2008), although this could increase significantly when exposed to harder radiation fields in low-metallicity environments ($\sim 20\%$, Peimbert et al. 2000). Therefore, the total argon abundance could be derived using an ionisation correction factor to account for the contribution of Ar³⁺ (e.g. Vermeij & van der Hulst 2002; Pérez-Montero et al. 2007; Hägele et al. 2008).

In combination with the low-resolution mode (LR, $R \sim 300$) of SAFARI, it would be also possible to obtain a direct determination of the neon abundance for star forming galaxies up to $z \sim 3$, based on the [Ne II]_{12.8μm} and [Ne III]_{15.6μm} lines. Ne²⁺ has a high ionisation potential (63.5 eV) above the helium absorption edge in stars (54.4 eV), and consequently Ne³⁺ does not exist in significant amounts (Bernard-Salas et al. 2009a; Hägele et al. 2008; Dors et al. 2013). At the lower end, neutral neon could exist within the Strömgren ra-

dus due to its relatively high ionisation potential (21.6 eV). However, a further investigation using photoionisation models proved that the expected amount of Ne⁰ within the nebula is negligible, with an ionisation correction factor below $\lesssim 1.05$ for a wide range of ionisation parameter values (Martín-Hernández et al. 2002). In the case of sulphur, a minor contribution of S⁴⁺ is expected due to the high ionisation potential of S³⁺ (47.3 eV), however S⁺ has an ionisation potential of 23.3 eV and thus it could be present in the nebula. Based on measurements of the sulphur abundance in nearby star forming regions (Peimbert 2003; Vermeij & van der Hulst 2002; García-Rojas et al. 2006) and photoionisation models (Tsamis & Péquignot 2005), the expected amount of S⁺ is less than $\sim 10\%$ of the total sulphur abundance (Leboutteiller et al. 2008; Bernard-Salas et al. 2009a). As in the case of argon, the gas-phase abundance of sulphur could be derived from the [S III]_{18.7μm} and [S IV]_{10.5μm} lines and the hydrogen recombination lines detected by SMI and SAFARI, using a relatively small ionisation correction factor.

In nearby galaxies, direct abundances could be determined using the *Huα* line (e.g. Bernard-Salas et al. 2009a), covered by SMI at high-spectral resolution (HR, $R \approx 28000$). As mentioned earlier, the weak dependence of the IR lines with the density and the effect of the radiation field hardness could be constrained using the corresponding diagnostics based on ratios of mid- and far-IR lines (e.g. Croxall et al. 2013). Besides argon, neon, and sulphur, we would be able to provide abundances for the dominant ionic species of nitrogen (N⁺ and N²⁺) and help in the determination of direct abundances for oxygen (O⁰, O²⁺, and O³⁺), iron (Fe⁺ and Fe²⁺), and carbon (C⁺), based on the spectral range covered by SMI and SAFARI ([N II]_{122μm} and [N III]_{57μm}; [O I]_{63,145μm}, [O III]_{52,88μm}, and [O IV]_{25.9μm}; [Fe II]_{17.9,26.0μm} and [Fe III]_{22.9μm}; [C II]_{158μm}).

3.3 The O₃N₃ index

One of the main IR diagnostics to measure the metallicity of galaxies is based on the ratio of the [O III]_{52,88μm} to [N III]_{57μm} lines. These are two key elements in the gas chemistry: oxygen is an alpha-capture primary element produced by massive stars, whereas nitrogen behaves as both a primary and a secondary nucleosynthetic element. As a result, the N/O relative abundance shows a dependence with the star-formation history of the galaxy, and the subsequent global metallicity (Liang et al. 2006; Pilyugin et al. 2014; Vincenzo et al. 2016), which could be determined by *SPICA* (Nagao et al. 2011; Pereira-Santaella et al. 2017). O and N have similar ionisation potentials for their first five ionisation stages and, thus, both have very similar ionisation structures almost independent of the ionisation parameter and hardness of the radiation field. Therefore, although ratios of [O III] to [N III] lines only trace the relative abundance of O²⁺ to N²⁺, this ratio serves as a very good proxy for the global N/O abundance ratio (see Pérez-Montero & Contini 2009 for a calibration using the optical [N II] λ6584/[O II] λ3727 line

ratio. The [O III] lines at 52 and 88 μm , whose ratio can be used as a density tracer for the ionised gas in the $\sim 10^2$ – 10^3 cm^{-3} range, are combined to produce a tracer for the gas metallicity with a weak dependency on the density. This tracer is based on the ratio of $(2.2 \times [\text{O III}]_{88\mu\text{m}} + [\text{O III}]_{52\mu\text{m}})$ to $[\text{N III}]_{57\mu\text{m}}$ (hereafter the O_3N_3 index), as shown by the top panel in Fig. 3, it can be applied to both starburst galaxies and AGN, almost unaffected by the temperature, the extinction, the density, and the hardness of the radiation field (for further details see Pereira-Santaella et al. 2017).

Gas metallicities can be determined using the diagnostic shown in Fig. 3 up to $z \sim 1.6$, where the $[\text{O III}]_{88\mu\text{m}}$ line would still fall within the spectral range of SAFARI (35–230 μm). A diagnostic based on the $[\text{O III}]_{52\mu\text{m}}/[\text{N III}]_{57\mu\text{m}}$ ratio (see Nagao et al. 2011) is also a metallicity tracer up to $z \sim 3$ if the density is constrained through other line ratios, e.g. from the $[\text{S III}]_{18.7,33.5\mu\text{m}}$ or the $[\text{Ne III}]_{15.6,36.0\mu\text{m}}$ lines. As shown in Fig. 2, a telescope like SPICA would be sensitive enough to detect these lines in a few hours of observing time in typical starburst galaxies and AGN with luminosities close to the knee of the luminosity function at $z \sim 3$.

3.4 The $\text{Ne}_{23}\text{S}_{34}$ index

Above $z \gtrsim 0.15$ and 0.7 , the $[\text{S IV}]_{10.5\mu\text{m}}$ line would enter in the SMI/HR and MR ranges, respectively, enabling an additional indirect abundance diagnostic – based on the calibration of metallicity-sensitive line ratios – using the $([\text{Ne II}]_{12.8\mu\text{m}} + [\text{Ne III}]_{15.6\mu\text{m}})$ to $([\text{S III}]_{18.7\mu\text{m}} + [\text{S IV}]_{10.5\mu\text{m}})$ line ratio (hereafter the $\text{Ne}_{23}\text{S}_{34}$ index; lower panel in Fig. 3; see Fernández-Ontiveros et al. 2016 for further details). The chemical species of Ne^+ and Ne^{2+} on one hand, and S^{2+} and S^{3+} on the other, are the most important stages of ionisation for neon and sulphur, respectively, in starburst galaxies and AGN. However, the stagnation of the sulphur abundance, possibly caused by depletion of sulphur onto dust grains (Verma et al. 2003; Dors et al. 2016; Vidal et al. 2017), prevent the rise of the sulphur line intensities with increasing metallicity. Thus, the total $[\text{S IV}]_{10.5\mu\text{m}} + [\text{S III}]_{18.7\mu\text{m}}$ remains almost constant, while the $[\text{Ne III}]_{15.6\mu\text{m}} + [\text{Ne II}]_{12.8\mu\text{m}}$ increases with the neon abundance, which is not depleted onto dust grains.

The bottom panel in Fig. 3 shows a calibration of this metallicity sensitive ratio obtained from *Spitzer*/IRS spectra in the high-resolution mode ($R \sim 600$) vs. gas-metallicities obtained from indirect optical tracers for a sample of unobscured local starburst and dwarf galaxies (Moustakas et al. 2010, Pilyugin et al. 2014). The blue shaded area corresponds to photoionisation models obtained with CLOUDY simulations (Ferland et al. 2017) for a starburst galaxy, assuming a constant sulphur abundance above $Z = 0.2 Z_\odot$, while the neon abundance increases linearly with the overall gas metallicity (see Fernández-Ontiveros et al. 2016 for a full description of these models). Both the theoretical predictions and the measurements of unobscured starburst and dwarf galaxies are in agreement, since the trend

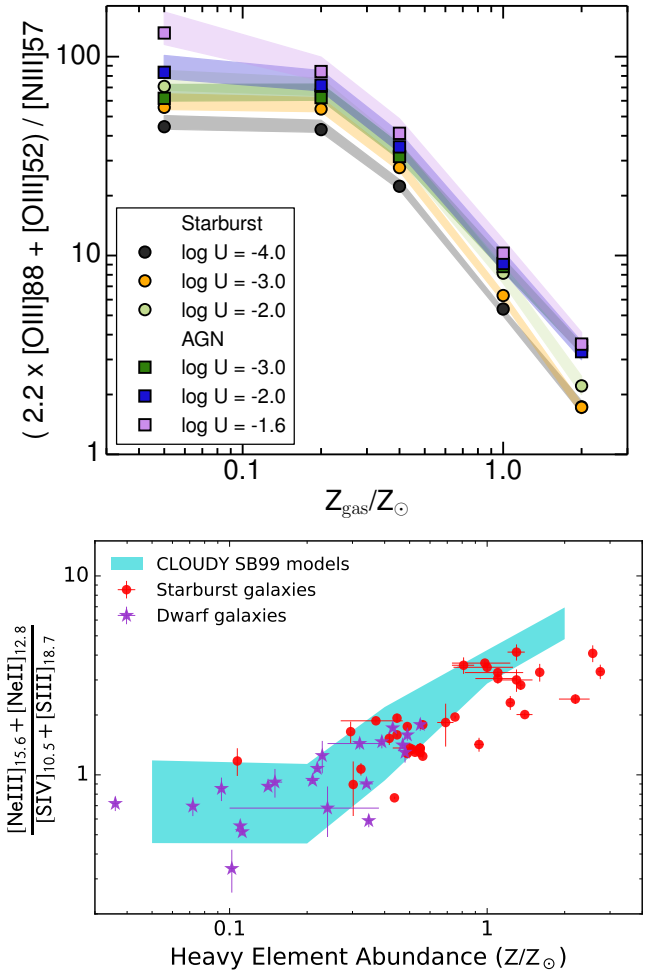


Figure 3. *Top:* AGN and starburst models for the metallicity sensitive $(2.2 \times [\text{O III}]_{88\mu\text{m}} + [\text{O III}]_{52\mu\text{m}}) / [\text{N III}]_{57\mu\text{m}}$ line ratio as a function of the gas-phase metallicity. For each metallicity bin, those models with the same ionisation parameter but different densities are grouped and their median ratio is indicated by a circle (square) for the starburst (AGN) models. The shaded area represents the scatter due to the gas density dependence of this ratio for a given ionisation parameter. Figure from Pereira-Santaella et al. (2017). *Bottom:* the $([\text{Ne II}]_{12.8\mu\text{m}} + [\text{Ne III}]_{15.6\mu\text{m}})$ to $([\text{S III}]_{18.7\mu\text{m}} + [\text{S IV}]_{10.5\mu\text{m}})$ line ratio (i.e. the $\text{Ne}_{23}\text{S}_{34}$ index) from *Spitzer*/IRS observations of starburst galaxies in the Local Universe vs. indirect gas-phase metallicity determined from strong optical lines (Moustakas et al. 2010; Pilyugin et al. 2014). The CLOUDY simulations including sulphur stagnation above $Z > 1/5 Z_\odot$ are in agreement with the observed increase of the line ratio with increasing metallicity for $Z \gtrsim 0.2 Z_\odot$ (figure adapted from Fernández-Ontiveros et al. 2016). Below $\lesssim 0.2 Z_\odot$, direct abundances can be estimated using, e.g. the ratio of $[\text{Ar II}]_{6.99\mu\text{m}}$ and $[\text{Ar III}]_{8.99\mu\text{m}}$ to the Pfund- α line for galaxies at $1.5 < z \leq 3$ (see Section 3.2).

shown by the models with sulphur abundance stagnation reproduces the behaviour of the observed line ratios. Since $[\text{Ne III}]$ and $[\text{Ne II}]$ are the most important stages of ionisation, the neon abundances determined with this method will be almost independent of ionisation correction factors.

All the lines used in this diagnostic would be covered by SMI and SAFARI for galaxies at $0.15 < z < 3$. The

weakest line in starburst galaxies with solar metallicities is $[\text{S IV}]_{10.5\mu\text{m}}$ (left panel in Fig. 2), although it is expected to become stronger with decreasing metallicity, as shown by the mid-IR spectra of low-metallicity dwarf galaxies in the Local Universe (e.g. Madden et al. 2006, Cormier et al. 2015). Therefore, high- z galaxies with sub-solar metallicities are expected to show stronger $[\text{S IV}]_{10.5\mu\text{m}}$ relative to other mid-IR fine-structure lines when compared to the spectrum of the starburst galaxy in Fig. 2. A different depletion pattern as that implied by Fig. 3 is not expected at high- z , since the range of metallicities probed by this diagram covers the range of values expected for galaxies at $z \lesssim 4$ (e.g. Davé et al. 2017). Still, this scenario could be explored using observations of the dust spectral features in the mid- to far-IR spectra of galaxies at high- z (see Section 4.3). At very low metallicities, studies based on galaxies in the Local Universe predict a constant N/O abundance ratio due to the primary origin of nitrogen in massive stars (van Zee et al. 1998), while sulphur does not show a significant abundance stagnation (Dors et al. 2016). Thus, both indirect tracers O_3N_3 and $\text{Ne}_{23}\text{S}_{34}$ show a flat behaviour below $\lesssim 0.2Z_\odot$ in Fig. 3. *SPICA* would be able to probe if this scenario holds at high- z . For instance, enhanced N/O abundances have been reported at $z \sim 2$ with regard to those of Local galaxies at similar gas-phase metallicities, possibly due to the high specific SFR at high- z (see discussion in Masters et al. 2014, 2016). On the other hand, direct abundance estimates for several ionic species can be obtained for neon, sulphur, oxygen, nitrogen, iron, and carbon below $0.2Z_\odot$ in galaxies at $1.5 < z \lesssim 3$, from ratios of the mid- and far-IR fine-structure lines of these elements to the Pfund- α line, covered by SMI/MR and SAFARI/LR (see Section 3.2; Fig. 2).

4 SPICA AND THE BUILD-UP OF METALS AND DUST

We discuss here the role that *SPICA* would play to address the science topics described in Section 2 – i.e. the assembly of galaxies, the evolution of metallicity in galaxies, and the build-up of cosmic dust – using the tracers for heavy element abundances and dust composition described in Section 3.

4.1 The Assembly of Galaxies

The potential of an observatory like *SPICA* to provide high-sensitivity IR spectral mapping of galaxies in the Local Universe, able to peer into their most obscured regions, would play an essential role to understand how galaxies were assembled. In the low-resolution mode, *SPICA* would be an extremely efficient mapping machine, reaching line luminosity noise levels of a few $10^{-19} \text{ W m}^{-2}$ over a square arcmin in less than a minute of observing time and over the entire wavelength range. Moreover, the 2.5 m mirror of *SPICA* would provide a diffraction-limited angular resolution of $\sim 2''$ to $32''$ in the 20–350 μm range, which corresponds to 100 pc–1.5 kpc at 10 Mpc, respectively. For example, this angular

resolution would be sufficient to resolve individual molecular clouds throughout galaxies in the Local Group (Milky Way, M31, M33, IC10, LMC, NGC 6822, SMC, and WLM, in order of decreasing metallicity). Metallicity determinations based on the O_3N_3 index could be obtained at $\sim 7''$ resolution ($\sim 0.3 \text{ kpc}$ at 10 Mpc), i.e. a fraction of about 1/100 of the diameter for a galaxy located at 10 Mpc with the size of the Milky Way. *SPICA* would be able to map a typical nearby spiral galaxy ($\sim 25 \text{ arcmin}^2$) with both SMI and SAFARI at medium to high-spectral resolution in about ~ 20 hours (see van der Tak et al. 2017).

The sensitivity and efficiency of an observatory like *SPICA* would allow us to quickly map large areas of nearby objects at the diffraction limit of the 2.5 m mirror above $\gtrsim 20 \mu\text{m}$. For instance, when compared with the *Herschel*/PACS spectral maps for NGC 891 (at 9.6 Mpc Hughes et al. 2015), *SPICA* would provide: *i*) about 100 times better sensitivity, thus revealing the outer galaxy regions with lower-surface brightness ($\sim 10^{-11} \text{ W m}^{-2} \text{ sr}^{-1}$, 5σ , 1 hr. compared to $\sim 5 \times 10^{-9} \text{ W m}^{-2} \text{ sr}^{-1}$ for the $[\text{O III}]_{88\mu\text{m}}$ line with PACS); *ii*) better spatial sampling ($\sim 0.5 \text{ kpc/pixel}$ in PACS); and *iii*) with a much larger efficiency to cover the full extension of NGC 891 ($\sim 7.7 \text{ arcmin}^2$) for the whole 12–230 μm spectral range in about 8 hr. – PACS measured small spectral windows centred on the $[\text{O I}]_{63,145\mu\text{m}}$, $[\text{O III}]_{88\mu\text{m}}$, $[\text{N II}]_{122\mu\text{m}}$, and $[\text{C II}]_{158\mu\text{m}}$ lines, covering half of this galaxy in a total of ~ 12 hours.

These capabilities would allow *SPICA* to trace the spatial distribution of heavy elements in ISM of nearby galaxies. The metal budget at different radii would be compared to the stellar metallicities, which can be derived from optical and near-IR spectroscopic studies (e.g. Coccato et al. 2013; Belfiore et al. 2016), and chemical evolution models. This approach would allow to estimate the average outflow loading factors over the galaxies lifetime – i.e. the ratio between the star formation and the mass outflow rates – which is an essential step to constrain the episodes of matter cycling, and ultimately to understand how nearby galaxies were assembled (see Belfiore et al. 2016; González-Alfonso et al. 2017). Therefore, a detailed study of the spatial distribution of heavy element abundances in nearby galaxies would be a unique probe of the past history in the evolution of these galaxies.

4.2 The Evolution of Metallicity in Galaxies

SPICA would be able to trace the global content of metals in galaxies from $z \sim 3$ till the present time. To accomplish this, future studies based on *SPICA* observations would dispose of heavy element abundances for galaxies up to $z \sim 3$, obtained from tracers with a feeble response to both extinction and temperature: e.g. using direct measurements of the main ionic species based on ratios of IR fine-structure lines to Pfund- α or $\text{H}\alpha$ and ionisation correction factors (see Section 3.2; Fig. 2); and/or indirect methods based on ratios of strong IR fine-structure lines such as those involved in the

O_3N_3 and the $\text{Ne}_{23}\text{S}_{34}$ indices (Sections 3.3 and 3.4, respectively; Fig. 3). A spectroscopic survey designed to observe thousand of galaxies at $z < 3$ – e.g. covering a wide range in luminosity, galaxy type – would allow to obtain a statistically valid assessment of the metallicity evolution in galaxies. *SPICA* would be able to accomplish such a survey in $\sim 4\,000$ hours of observing time.

Once the metallicities are measured using IR tracers, a global view of the baryon cycle could be derived by including the two remaining ingredients, i.e. the stellar mass and the total gas content of these galaxies. The latter would rely mainly on future and present facilities. For instance, the stellar mass can be obtained from near- and mid-IR photometric surveys available nowadays (e.g. with *AKARI*, Ishihara et al. 2010; *WISE*, Wright et al. 2010; *Spitzer*, Ashby et al. 2013), plus future catalogues assembled by the extremely-large telescopes (ELTs) – the European-ELT³, the Thirty Meter Telescope (Sanders 2013), and the Giant Magellan Telescope (Shethman & Johns 2010), *Euclid* (Maciaszek et al. 2016), the *Wide Field Infrared Survey Telescope* (*WFIRST*; Spergel et al. 2013), and available *James Webb Space Telescope* (*JWST*; Gardner et al. 2006) observations at the time. On the other hand, the molecular gas content can be derived from follow-up observations of these sources with the Atacama Large Millimeter/submillimeter Array (ALMA; Wootten & Thompson 2009) and the Northern Extended Millimeter Array (NOEMA⁴) in the CO and $[\text{C I}]_{371,609\mu\text{m}}$ transitions, assuming a conversion factor⁵ from CO or C I to H_2 (e.g. Papadopoulos & Greve 2004). Alternatively, a proxy for the molecular gas content could be inferred from the *SPICA* spectra using IR transitions sensitive to the SFR such as the neon lines (Ho & Keto 2007), or from the modelling of the 24–60 μm rest-frame continuum which is also sensitive to the SFR (Ciesla et al. 2014; van der Tak et al. 2017). To remove the possible AGN contamination, the relative AGN/starburst contribution could be derived from the ratio of $[\text{O IV}]_{25.9\mu\text{m}}$ to either $[\text{O III}]_{52,88\mu\text{m}}$ or the total $[\text{Ne II}]_{12,8\mu\text{m}} + [\text{Ne III}]_{15,6\mu\text{m}}$ (Spinoglio et al. 2015; Fernández-Ontiveros et al. 2016). Finally, the atomic gas content could be estimated from observations in the H I line, e.g. using the Square Kilometer Array (SKA; Dewdney et al. 2009), which will be already operational by the mid-2020s, though fully developed at the end of the decade.

4.3 The Build-Up of Cosmic Dust

The unique sensitivity of a cryogenic telescope with the characteristics of *SPICA* would enable the study of the dust composition based on several spectral features in the mid- to

far-IR range (Section 3.1; van der Tak et al. 2017), largely improving the work based on *Spitzer* and *Herschel* spectroscopic observations (e.g. Spoon et al. 2006; Matsuura et al. 2015). A whole new suite of solid-state features can be used to investigate the main sources of dust in the ISM of galaxies at high- z . Among the different sources that contribute to the dust reservoir in galaxies one can find: evolved stars, producing crystalline silicates (Molster et al. 1999, 2002), dolomite and calcite (Kemper et al. 2002), and complex carbon molecules such as C_{60} and C_{70} (Cami et al. 2010); post-AGB stars show a rich IR spectrum, as shown by Matsuura et al. (2014), with features at 15.8 μm and 21 μm (associated with PAHs), and 30 μm (ascribed to MgS); supernovae remnants (SNR) may also be a significant source of dust at high- z , e.g. Cassiopeia A shows a prominent 21 μm feature associated with FeO and possibly SiO_2 (Rho et al. 2008).

In nearby galaxies, medium and high-resolution spectroscopy with SMI and SAFARI would be able to resolve the emission of SNR from the surrounding ISM at ~ 1 Mpc (assuming a SNR size of ~ 60 pc; Elwood et al. 2017) and investigate the properties and composition of the surviving dust after the pass of the reverse shock. Only far-IR follow-up observations of SNR in the Local Universe can probe the dust composition and size distribution produced by these sources. Specifically, future observations of SN 1987A would be of particular interest to constrain current models of dust condensation efficiency after the passage of the reverse shock. A detailed discussion on the role of *SPICA* in the study of dust properties in nearby galaxies can be found in the companion paper by van der Tak et al. (2017).

Focusing on studies at high- z , a cryogenic IR observatory like *SPICA* would be sensitive enough to distinguish among different shapes in the rest-frame mid-IR spectrum of galaxies associated with differences in the chemical composition of dust. The predicted shape of the mid- to far-IR spectra for three quasars with different dust compositions, from the results of Xie et al. (2017), are shown in Fig. 4 scaled to a luminosity of $2 \times 10^{12} L_{\odot}$. The dust composition determines the central wavelength, width, and relative intensity of the two silicate bands at 9.7 μm and 18 μm . Thus, a detailed modelling of the continuum emission and the dust emission and absorption features in this range is able to probe the dust composition (e.g. Spoon et al. 2006). The quasar spectra shown in Fig. 4 are dominated by astronomical silicate (PG 1004+130, in red), amorphous olivine (PG 1351+640, in yellow), and amorphous pyroxene (PG 2214+139, in pink). Therefore, the access to dust features in the rest-frame mid- to far-IR range with *SPICA* would allow us to explore, for the first time, the composition of dust in galaxies at the peak of the star formation and SMBH accretion activity ($1 < z < 3$). At farther distances, $z \gtrsim 4$, very little is known on the dust produced by metal-free SNe (Nozawa et al. 2003; Schneider et al. 2004), which could be investigated through mid-IR bands such as those produced by magnetite (Fe_3O_4), as discussed in a forthcoming study by Egami et al. (in preparation).

³<http://www.eso.org/sci/facilities/eelt/>

⁴<http://www.iram-institute.org/EN/noema-project.php>

⁵The dependence of this conversion factor with metallicity (e.g. Schrubba et al. 2012) could be calibrated for nearby galaxies using both the HD lines at 56 and 112 μm and the $[\text{C II}]_{158\mu\text{m}}$ line to detect CO-dark gas (see van der Tak et al. 2017). *SPICA* would detect the HD lines in typical galaxies up to ~ 10 Mpc.

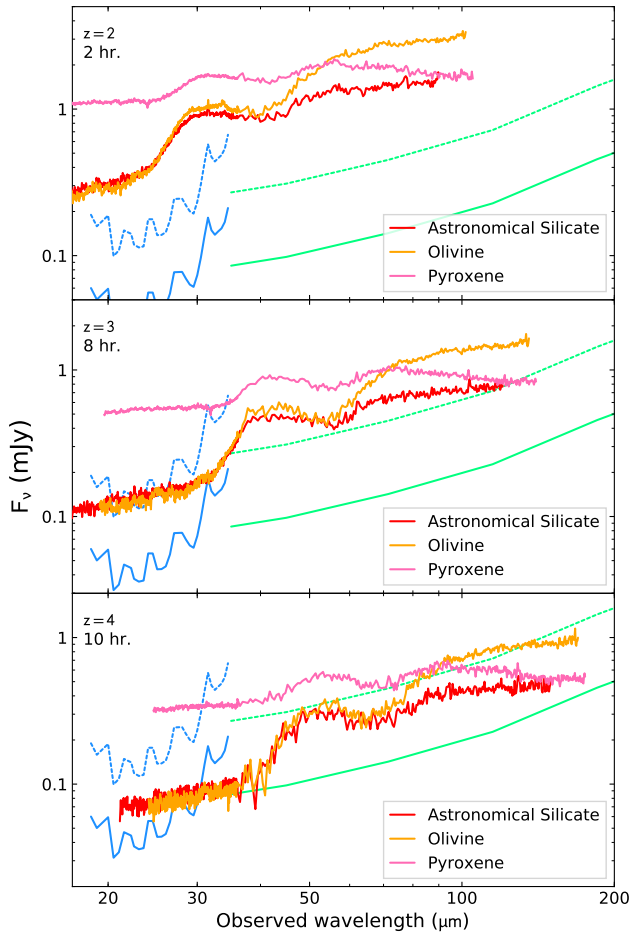


Figure 4. Differences in the *Spitzer*/IRS spectrum of three quasars associated to different silicate compositions (see Xie et al. 2017): PG 1004+130 (astronomical silicate, in red colour), PG 1351+640 (amorphous olivine, in yellow), and PG 2214+139 (amorphous pyroxene, in pink). In this simulation the spectra have been scaled to a luminosity of $10^{12} L_{\odot}$, and located at $z = 2$ (top panel, 2 hours of integration time), $z = 3$ (central panel, 8 hours), and $z = 4$ (bottom panel). The *SPICA* 5σ sensitivities for SMI/MR (in blue) and SAFARI/LR (in green) are indicated for integration times of 1 hour (dotted lines) and 10 hours (solid lines).

Finally, other agents involved in the baryon cycle can have a strong influence in the dust content and composition. For instance, outflows originated by AGN and star formation activity can remove dust from the ISM, while inflows from the halo and the IGM surrounding the galaxy can alter the dust content and composition (Ciesla et al. 2015; González-Alfonso et al. 2017). Only an IR observatory with the characteristics of *SPICA* could determine the impact of these processes in the ISM chemistry.

5 Synergies with Future Facilities

SPICA is planned for the late 2020s, during a lively period for multi-wavelength astronomy and galaxy evolution studies in

particular. However, the observations that would be provided by *SPICA* are not accessible to any of the future generation of ground-based ELTs nor to *JWST*. These facilities will have access to the rest-frame optical and near-IR spectra of high- z galaxies ($z \gtrsim 1$) with a limited access to the mid-IR range ($\lambda \lesssim 7 \mu\text{m}$ at $z = 3$). Therefore, the use of IR tracers based on *JWST* and ELTs observations will be restricted to galaxies in the Local and nearby ($z < 0.5$) Universe.

At the time *SPICA* will fly, the catalogues delivered by *Euclid* and *WFIRST* in the near-IR, by the *Advanced Telescope for High Energy Astrophysics (Athena+; Nandra et al. 2013)* in the X-ray range, will be already available, containing a vast number of sources at $1 < z < 3$. Together with the galaxies that would be eventually discovered by a spectrophotometric survey with SMI in the mid-IR (see Gruppioni et al. 2017), these catalogues would be useful to define a sample of galaxies to study the chemical evolution over cosmic time. This sample would be observed with mid- to high resolution spectroscopy using SMI and SAFARI. From these catalogues, *SPICA* would be able to identify candidates to perform follow-up spectroscopic observations in the mid- to far-IR rest-frame range with medium resolution ($R \gtrsim 300$) SAFARI and SMI. These observations could be the basis for the study of the chemical evolution of galaxies (see Section 4.2). Of particular interest in this field are the synergies of SMI and SAFARI spectroscopy with the Mid-InfraRed Instrument (MIRI) on-board *JWST*. The latter could provide abundance determinations for the main ionic species of several elements (see Section 3.1) in galaxies at $1 < z \lesssim 3$ based on the combination of $\text{Br}\alpha$ ($4.051 \mu\text{m}$ in the rest-frame), $\text{Pa}\alpha$ ($1.875 \mu\text{m}$), and $\text{Pa}\beta$ ($1.282 \mu\text{m}$) with *JWST* and the fine-structure lines of the chemical species in the mid- to far-IR range provided by *SPICA*. On the other hand, far-IR lines such as $[\text{N II}]_{57\mu\text{m}}$ and $[\text{N III}]_{122\mu\text{m}}$ would provide an abundance estimate for the main ionisation stages of nitrogen, when coupled with the hydrogen recombination lines in the near-IR provided by *JWST*.

The synergy between *SPICA* and *Athena+* would allow us to address the problem of the “missing metals” in galaxies at high- z . When compared to the estimates based on the cosmic star-formation history, current observations of galaxy populations at $z \sim 2.5$ are missing about half of the heavy element abundances expected (Bouché et al. 2007; Gallazzi et al. 2008). *SPICA* would reveal the metal content of the dust-embedded star formation, which is missing in optically-based abundance measurements (Santini et al. 2010). Still, a large fraction of metals are possibly locked in the hot intracluster gas (Ferrara et al. 2005; Davé & Oppenheimer 2007), which is chemically enriched with the gas removed from galaxies by processes such as outflows – driven by star formation or AGN – or ram-pressure stripping. *Athena+* will be able to measure the abundances and distribution of metals in clusters from the core to the boundary of the virial regions (Nandra et al. 2013). Furthermore, the study of the dust composition in galaxies using IR spectroscopy with *SPICA* could be complemented with the dust mineralogy obtained with *Athena+*

from the analysis of X-ray absorption edges produced by chemical elements trapped into dust grains (e.g. Lee & Ravel 2005; Hoffman & Draine 2016; Palmeri et al. 2016). Thus, the combination of these two observatories would provide a accurate measurement of the metal budget in galaxies and the ICM from $z \sim 3$ till the present time.

Additionally, chemical evolution models could be constrained by including the content of the molecular and neutral gas with the help of ALMA and SKA, respectively, as mentioned in Section 4.2. The latter will be of particular interest to understand the matter cycle and the build-up and evolution of the metallicity relations found from high- z galaxies to the Local Universe (see Section 2.2). On the other hand, the combined work of *SPICA* and ALMA could follow the highly successful synergy between *Spitzer* and *Herschel* at low- z to cover both sides of the dust thermal emission. These facilities would provide dust masses and temperatures for distant galaxies (see Gruppioni et al. 2017), as *Herschel* did on nearby galaxies and a few of the brighter galaxies at high- z (e.g. Magdis et al. 2012).

6 SUMMARY

One of the major challenges in astronomy for the next ~ 20 years is to understand the cycle of matter within galaxies and identify the physical mechanisms driving their evolution. This task can only be addressed from a multi-wavelength point of view, and thus will require the use of a sensitive IR spectroscopic observatory combined with the main observatories available in the next decades including *JWST*, the ELTs, *Athena+*, ALMA, NOEMA, SKA, but also the survey capabilities of, e.g. *Euclid* and *WFIRST*. The contribution of *SPICA* would be essential to study the chemical evolution of galaxies, which is one of the most important manifestations of the baryon cycle activity in galaxies. The past history of gas accretion, star formation, nuclear activity, and gas outflows leaves an imprint on the composition and content of heavy elements and dust in the ISM of galaxies. Thus, metals and dust are relics through which one can reconstruct the evolutionary path that galaxies have followed from their formation to the present time.

The 2.5 m actively cooled mirror of *SPICA* (~ 6 K) would reach a unique sensitivity allowing the observation of the whole suite of lines and dust features in the rest-frame mid- and far-IR range, from the faintest regions in nearby galaxies to the knee of the luminosity function at the peak of star formation and black hole accretion activity ($1 < z < 3$). *SPICA* would play a major role to unveil the dark side of galaxy evolution, since the bulk of star formation and black hole accretion can only be attained at long IR wavelengths (Spinoglio et al. 2017). While *JWST* will probe the external parts of high- z galaxies through rest-frame optical/UV spectra, and ALMA will study the cold gas reservoir, the contribution of *SPICA* would be essential to provide an insight into the warm gas in the dust-enshrouded regions of galaxies. No other facility with similar capabilities is currently planned.

Therefore, rest-frame mid- to far-IR spectroscopy is essential to understand the physical processes at the engine of the matter cycle in galaxies.

Only a deep survey of spectroscopic observations with a sensitive IR observatory like *SPICA* would reveal the chemical enrichment process for galaxies in the last ~ 11 Gyr. When combined with present and forthcoming first-line facilities in the decade of the 2020s, this spectroscopic survey would allow us to determine the evolutionary path followed by galaxies from the peak of star formation and SMBH accretion activity till the present time, and ultimately understand both the sequence of physical mechanisms involved in the matter cycle and how they drive the evolution of galaxies over cosmic time.

In this work we evaluate the feasibility of the main observational strategies foreseen to derive heavy element abundances and trace the dust composition in galaxies accessible to *SPICA*, from high- z to the Local Universe. IR diagnostics offer a huge advantage over optical/UV line ratios, since IR line intensities show a feeble response to both extinction by dust and gas temperature. Under the light of these tools, we also explore the potential contribution of an observatory with the characteristics of *SPICA* to address some of the main questions in the field of galaxy evolution that will be unanswered in the late 2020s: how are galaxies assembled? How is the build-up of metals and dust? And how does the ISM composition evolve with redshift? The use of IR diagnostics applied to large spectroscopic samples would yield a unique view of the chemical evolution in galaxies, a key contribution to understand the picture provided by future studies based on *JWST*, ALMA, and ELTs observations in the 2020s.

7 ACKNOWLEDGEMENTS

This paper is dedicated to the memory of Bruce Swinyard, who initiated the *SPICA* project in Europe, but unfortunately died on 22 May 2015 at the age of 52. He was *ISO-LWS* calibration scientist, *Herschel-SPIRE* instrument scientist, first European PI of *SPICA* and first design lead of SAFARI.

The SAFARI Consortium and the full *SPICA* Team are acknowledged, without their work this mission project would not have been possible. J.A.F.O. acknowledges financial support from the Spanish Ministry of Economy and Competitiveness (MINECO) under grant number MEC-AYA2015-53753-P.

Affiliations

- ¹Instituto de Astrofísica de Canarias (IAC), C/Vía Láctea s/n, E-38205 La Laguna, Spain
- ²Universidad de La Laguna (ULL), Dept. de Astrofísica, Avd. Astrofísico Fco. Sánchez s/n, E-38206 La Laguna, Spain
- ³Istituto di Astrofisica e Planetologia Spaziali (INAF-IAPS), Via Fosso del Cavaliere 100, I-00133 Roma, Italy
- ⁴IPAC, California Institute of Technology, Pasadena, CA 91125, USA
- ⁵Sterrenkundig Observatorium, Universiteit Gent, Krijgslaan 281 S9, 9000 Gent, Belgium
- ⁶Department of Physical Sciences, The Open University, MK7 6AA, Milton Keynes, United Kingdom
- ⁷Department of Astronomy and Joint Space Institute, University of Maryland, College Park, MD 20642 USA

⁸Laboratoire d'Astrophysique de Bordeaux, Univ. Bordeaux, CNRS, B18N, allée Geoffroy Saint-Hilaire, 33615 Pessac, France

⁹Laboratoire AIM, CEA/IRFU/Service d'Astrophysique, Université Paris Diderot, Bat. 709, F-91191 Gif-sur-Yvette, France

¹⁰Department of Physics and Astronomy, University College London, Gower Street, London WC1E 6BT, UK

¹¹Steward Observatory, University of Arizona, 933 North Cherry Avenue, Tucson, AZ 85721, USA

¹²Naval Research Laboratory, Remote Sensing Division, 4555 Overlook Avenue SW, Washington DC 20375, USA

¹³CNRS, IRAP, 9 Av. colonel Roche, BP 44346, 31028 Toulouse Cedex 4, France

¹⁴Université de Toulouse, UPS-OMP, IRAP, 31028 Toulouse Cedex 4, France

¹⁵Universidad de Alcalá, Dept. de Física y Matemáticas, Campus Universitario, E-28871 Alcalá de Henares, Madrid, Spain

¹⁶Osservatorio Astronomico di Trieste, INAF, Via Tiepolo 11, I-34131 Trieste, Italy

¹⁷Osservatorio Astronomico di Bologna, INAF, via Ranzani 1, I-40127 Bologna, Italy

¹⁸National Astronomical Observatory of Japan, 2-21-1 Osawa, Mitaka, Tokyo 181-8588, Japan

¹⁹Graduate School of Science, Nagoya University, Furo-cho, Chikusa-ku, Nagoya 464-8602, Japan

²⁰Astronomy Division, University of California, Los Angeles, CA 90095-1547, USA

²¹Institute of Space Astronautical Science, Japan Aerospace Exploration Agency, Sagami-hara, Kanagawa 252-5210, Japan

²²School of Physics and Astronomy, Cardiff University, Queen's Buildings, The Parade, Cardiff CF24 3AA, United Kingdom

²³Research Center for Space and Cosmic Evolution, Ehime University, Matsuyama 790-8577, Japan

²⁴Centro de Astrobiología (CSIC/INTA), Ctra. de Ajalvir km. 4, 28850 Torrejón de Ardoz, Madrid, Spain

²⁵Department of Astronomy, Graduate School of Science, The University of Tokyo, 113-0033 Tokyo, Japan

²⁶Department of Physics, University of Oxford, Oxford OX1 3RH, UK

²⁷SRON Netherlands Institute for Space Research, Postbus 800, 9700, AV Groningen, The Netherlands

²⁸Kapteyn Astronomical Institute, University of Groningen, Postbus 800, 9700 AV, Groningen, The Netherlands

²⁹Osservatorio Astronomico di Roma, INAF, Via di Frascati 33, I-00078 Monte Porzio Catone, Italy

³⁰Ritter Astrophysical Research Center, University of Toledo, 2825 West Bancroft Street, M. S. 113, Toledo, OH 43606, USA

³¹International Research Fellow of the Japan Society for the Promotion of Science (JSPS), Department of Astronomy, University of Tokyo, Bunkyo-ku, 113-0033 Tokyo, Japan

REFERENCES

- Abel N. P., Dudley C., Fischer J., Satyapal S., van Hoof P. A. M., 2009, *ApJ*, **701**, 1147
- Andrews B. H., Martini P., 2013, *ApJ*, **765**, 140
- Anglés-Alcázar D., Davé R., Özel F., Oppenheimer B. D., 2014, *ApJ*, **782**, 84
- Asano R. S., Takeuchi T. T., Hirashita H., Inoue A. K., 2013a, *Earth, Planets, and Space*, **65**, 213
- Asano R. S., Takeuchi T. T., Hirashita H., Nozawa T., 2013b, *MNRAS*, **432**, 637
- Ashby M. L. N., et al., 2013, *ApJ*, **769**, 80
- Bakes E. L. O., Tielens A. G. G. M., 1994, *ApJ*, **427**, 822
- Bakes E. L. O., Tielens A. G. G. M., 1998, *ApJ*, **499**, 258
- Belfiore F., Maiolino R., Bothwell M., 2016, *MNRAS*, **455**, 1218
- Bernard-Salas J., Pottasch S. R., Beintema D. A., Wesselius P. R., 2001, *A&A*, **367**, 949
- Bernard-Salas J., et al., 2009a, *ApJS*, **184**, 230
- Bernard-Salas J., Peeters E., Sloan G. C., Gutenkunst S., Matsuura

M., Tielens A. G. G. M., Zijlstra A. A., Houck J. R., 2009b, *ApJ*, **699**, 1541

Borkowski K. J., Harrington J. P., 1991, *ApJ*, **379**, 168

Bothwell M. S., Maiolino R., Kennicutt R., Cresci G., Mannucci F., Marconi A., Cicone C., 2013, *MNRAS*, **433**, 1425

Bothwell M. S., Maiolino R., Peng Y., Cicone C., Griffith H., Wagg J., 2016a, *MNRAS*, **455**, 1156

Bothwell M. S., Maiolino R., Cicone C., Peng Y., Wagg J., 2016b, *A&A*, **595**, A48

Bouché N., Lehnert M. D., Aguirre A., Péroux C., Bergeron J., 2007, *MNRAS*, **378**, 525

Boyle B. J., Terlevich R. J., 1998, *MNRAS*, **293**, L49

Bresolin F., Schaerer D., González Delgado R. M., Stasińska G., 2005, *A&A*, **441**, 981

Brisbin D., Ferkinhoff C., Nikola T., Parshley S., Stacey G. J., Spoon H., Hailey-Dunsheath S., Verma A., 2015, *ApJ*, **799**, 13

Brooks A. M., Governato F., Booth C. M., Willman B., Gardner J. P., Wadsley J., Stinson G., Quinn T., 2007, *ApJ*, **655**, L17

Brooks A. M., Governato F., Quinn T., Brook C. B., Wadsley J., 2009, *ApJ*, **694**, 396

Cami J., Bernard-Salas J., Peeters E., Malek S. E., 2010, *Science*, **329**, 1180

Ciesla L., et al., 2014, *A&A*, **565**, A128

Ciesla L., et al., 2015, *A&A*, **576**, A10

Clegg R. E. S., Harrington J. P., 1989, *MNRAS*, **239**, 869

Coccatto L., Morelli L., Pizzella A., Corsini E. M., Buson L. M., Dalla Bontà E., 2013, *A&A*, **549**, A3

Cormier D., et al., 2015, *A&A*, **578**, A53

Croxall K. V., et al., 2013, *ApJ*, **777**, 96

Davé R., Oppenheimer B. D., 2007, *MNRAS*, **374**, 427

Davé R., Finlator K., Oppenheimer B. D., 2011, *MNRAS*, **416**, 1354

Davé R., Finlator K., Oppenheimer B. D., 2012, *MNRAS*, **421**, 98

Davé R., Rafieferantsoa M. H., Thompson R. J., Hopkins P. F., 2017, *MNRAS*, **467**, 115

Delgado Inglada G., Rodríguez M., Mampaso A., Viironen K., 2009, *ApJ*, **694**, 1335

Dewdney P. E., Hall P. J., Schilizzi R. T., Lazio T. J. L. W., 2009, *IEEE Proceedings*, **97**, 1482

Dopita M. A., Kewley L. J., Sutherland R. S., Nicholls D. C., 2016, *Ap&SS*, **361**, 61

Dors Jr. O. L., Copetti M. V. F., 2005, *A&A*, **437**, 837

Dors O. L., et al., 2013, *MNRAS*, **432**, 2512

Dors O. L., Cardaci M. V., Hägele G. F., Krabbe A. C., 2014, *MNRAS*, **443**, 1291

Dors O. L., Pérez-Montero E., Hägele G. F., Cardaci M. V., Krabbe A. C., 2016, *MNRAS*, **456**, 4407

Draine B. T., 2003, *ARA&A*, **41**, 241

Draine B. T., 2011, *Physics of the Interstellar and Intergalactic Medium*. Princeton University Press

Dulieu F., Congiu E., Noble J., Baouche S., Chaabouni H., Moudens A., Minissale M., Cazaux S., 2013, *Scientific Reports*, **3**, 1338

Elwood B. D., Murphy J. W., Diaz M., 2017, preprint, ([arXiv:1701.07057](https://arxiv.org/abs/1701.07057))

Ferland G. J., et al., 2017, *RMxAA*, **53**, 385

Fernández-Ontiveros J. A., Spinoglio L., Pereira-Santaella M., Malkan M. A., Andreani P., Dasyra K. M., 2016, *ApJS*, **226**, 19

- Ferrara A., Scannapieco E., Bergeron J., 2005, *ApJ*, **634**, L37
- Finlator K., Davé R., 2008, *MNRAS*, **385**, 2181
- Fischer J., Abel N. P., González-Alfonso E., Dudley C. C., Satyapal S., van Hoof P. A. M., 2014, *ApJ*, **795**, 117
- Franceschini A., Hasinger G., Miyaji T., Malquori D., 1999, *MNRAS*, **310**, L5
- Fu J., Hou J. L., Yin J., Chang R. X., 2009, *ApJ*, **696**, 668
- Gallazzi A., Charlot S., Brinchmann J., White S. D. M., 2006, *MNRAS*, **370**, 1106
- Gallazzi A., Brinchmann J., Charlot S., White S. D. M., 2008, *MNRAS*, **383**, 1439
- García-Rojas J., Esteban C., Peimbert M., Costado M. T., Rodríguez M., Peimbert A., Ruiz M. T., 2006, *MNRAS*, **368**, 253
- Gardner J. P., et al., 2006, *Space Sci. Rev.*, **123**, 485
- González-Alfonso E., et al., 2015, *ApJ*, **800**, 69
- González-Alfonso E., et al., 2017, *PASA*, this issue
- González Delgado R. M., et al., 2015, *A&A*, **581**, A103
- Graciá-Carpio J., et al., 2011, *ApJ*, **728**, L7
- Gruppioni C., et al., 2017, *PASA*, this issue
- Hägele G. F., Díaz A. I., Terlevich E., Terlevich R., Pérez-Montero E., Cardaci M. V., 2008, *MNRAS*, **383**, 209
- Ho L. C., Keto E., 2007, *ApJ*, **658**, 314
- Hoffman J., Draine B. T., 2016, *ApJ*, **817**, 139
- Hughes T. M., et al., 2015, *A&A*, **575**, A17
- Hunt L., Dayal P., Magrini L., Ferrara A., 2016a, *MNRAS*, **463**, 2002
- Hunt L., Dayal P., Magrini L., Ferrara A., 2016b, *MNRAS*, **463**, 2020
- Ishihara D., et al., 2010, *A&A*, **514**, A1
- Izotov Y. I., Thuan T. X., 1999, *ApJ*, **511**, 639
- Izotov Y. I., Thuan T. X., Lipovetsky V. A., 1994, *ApJ*, **435**, 647
- Izotov Y. I., Thuan T. X., Lipovetsky V. A., 1997, *ApJS*, **108**, 1
- Kaneda H., et al., 2017, *PASA*, submitted as part of this issue
- Kemper F., Jäger C., Waters L. B. F. M., Henning T., Molster F. J., Barlow M. J., Lim T., de Koter A., 2002, *Nature*, **415**, 295
- Kennicutt Jr. R. C., 1998, *ApJ*, **498**, 541
- Kennicutt Jr. R. C., Bresolin F., Garnett D. R., 2003, *ApJ*, **591**, 801
- Kewley L. J., Ellison S. L., 2008, *ApJ*, **681**, 1183
- Kewley L. J., Geller M. J., Barton E. J., 2006, *AJ*, **131**, 2004
- Koike C., Chihara H., Tsuchiyama A., Suto H., Sogawa H., Okuda H., 2003, *A&A*, **399**, 1101
- Köppen J., Weidner C., Kroupa P., 2007, *MNRAS*, **375**, 673
- Lara-López M. A., et al., 2010, *A&A*, **521**, L53
- Lebouteiller V., Kunth D., Lequeux J., Lecavelier des Etangs A., Désert J.-M., Hébrard G., Vidal-Madjar A., 2004, *A&A*, **415**, 55
- Lebouteiller V., Kunth D., Lequeux J., Aloisi A., Désert J.-M., Hébrard G., Lecavelier Des Étangs A., Vidal-Madjar A., 2006, *A&A*, **459**, 161
- Lebouteiller V., Bernard-Salas J., Brandl B., Whelan D. G., Wu Y., Charmandaris V., Devost D., Houck J. R., 2008, *ApJ*, **680**, 398
- Lee J. C., Ravel B., 2005, *ApJ*, **622**, 970
- Lequeux J., Peimbert M., Rayo J. F., Serrano A., Torres-Peimbert S., 1979, *A&A*, **80**, 155
- Liang Y. C., Yin S. Y., Hammer F., Deng L. C., Flores H., Zhang B., 2006, *ApJ*, **652**, 257
- Maciaszek T., et al., 2016, in *Society of Photo-Optical Instrumentation Engineers (SPIE) Conference Series*. p. 99040T, doi:10.1117/12.2232941
- Madau P., Dickinson M., 2014, *ARA&A*, **52**, 415
- Madden S. C., Galliano F., Jones A. P., Sauvage M., 2006, *A&A*, **446**, 877
- Magdis G. E., et al., 2012, *ApJ*, **760**, 6
- Mallik D. C. V., Peimbert M., 1988, *RMxAA*, **16**, 111
- Mancuso C., Lapi A., Shi J., Cai Z.-Y., Gonzalez-Nuevo J., Béthermin M., Danese L., 2016, *ApJ*, **833**, 152
- Mannucci F., Cresci G., Maiolino R., Marconi A., Gnerucci A., 2010, *MNRAS*, **408**, 2115
- Martín-Hernández N. L., et al., 2002, *A&A*, **381**, 606
- Masters D., et al., 2014, *ApJ*, **785**, 153
- Masters D., Faisst A., Capak P., 2016, *ApJ*, **828**, 18
- Matsuura M., et al., 2014, *MNRAS*, **439**, 1472
- Matsuura M., et al., 2015, *ApJ*, **800**, 50
- McGaugh S. S., 1991, *ApJ*, **380**, 140
- Molster F. J., et al., 1999, *Nature*, **401**, 563
- Molster F. J., Waters L. B. F. M., Tielens A. G. G. M., 2002, *A&A*, **382**, 222
- Moustakas J., Kennicutt Jr. R. C., Tremonti C. A., Dale D. A., Smith J.-D. T., Calzetti D., 2010, *ApJS*, **190**, 233
- Nagao T., Maiolino R., Marconi A., Matsuhara H., 2011, *A&A*, **526**, A149
- Nakagawa T., Shibai H., Onaka T., Matsuhara H., Kaneda H., Kawakatsu Y., Roelfsema P., 2014, in *Space Telescopes and Instrumentation 2014: Optical, Infrared, and Millimeter Wave*. p. 91431I, doi:10.1117/12.2055947
- Nandra K., et al., 2013, preprint, (arXiv:1306.2307)
- Nieva M.-F., Przybilla N., 2012, *A&A*, **539**, A143
- Nozawa T., Kozasa T., Umeda H., Maeda K., Nomoto K., 2003, *ApJ*, **598**, 785
- Omukai K., Tsuribe T., Schneider R., Ferrara A., 2005, *ApJ*, **626**, 627
- Oppenheimer B. D., Davé R., 2006, *MNRAS*, **373**, 1265
- Pagel B. E. J., Edmunds M. G., Blackwell D. E., Chun M. S., Smith G., 1979, *MNRAS*, **189**, 95
- Palmeri P., Quinet P., Mendoza C., Bautista M. A., Witthoef M. C., Kallman T. R., 2016, *A&A*, **589**, A137
- Papadopoulos P. P., Greve T. R., 2004, *ApJ*, **615**, L29
- Peebles M. S., Shankar F., 2011, *MNRAS*, **417**, 2962
- Peimbert A., 2003, *ApJ*, **584**, 735
- Peimbert A., Peimbert M., 2010, *ApJ*, **724**, 791
- Peimbert M., Peimbert A., Ruiz M. T., 2000, *ApJ*, **541**, 688
- Pereira-Santaella M., Rigopoulou D., Farrah D., Lebouteiller V., Li J., 2017, *MNRAS*, **470**, 1218
- Pérez-Montero E., Amorín R., 2017, *MNRAS*, **467**, 1287
- Pérez-Montero E., Contini T., 2009, *MNRAS*, **398**, 949
- Pérez-Montero E., Hägele G. F., Contini T., Díaz Á. I., 2007, *MNRAS*, **381**, 125
- Pettini M., Pagel B. E. J., 2004, *MNRAS*, **348**, L59
- Pilyugin L. S., 2001a, *A&A*, **369**, 594
- Pilyugin L. S., 2001b, *A&A*, **374**, 412
- Pilyugin L. S., Thuan T. X., 2005, *ApJ*, **631**, 231
- Pilyugin L. S., Grebel E. K., Kniazev A. Y., 2014, *AJ*, **147**, 131
- Popping G., Somerville R. S., Galametz M., 2017, *MNRAS*, **471**, 3152
- Rémy-Ruyer A., et al., 2014, *A&A*, **563**, A31

- Rémy-Ruyer A., et al., 2015, *A&A*, **582**, A121
- Rho J., et al., 2008, *ApJ*, **673**, 271
- Roelfsema P., et al., 2017, *A&A*, submitted
- Ruiz A., Risaliti G., Nardini E., Panessa F., Carrera F. J., 2013, *A&A*, **549**, A125
- Sanders G. H., 2013, *Journal of Astrophysics and Astronomy*, **34**, 81
- Santini P., et al., 2010, *A&A*, **518**, L154
- Schmidt M., 1959, *ApJ*, **129**, 243
- Schneider R., Ferrara A., Salvaterra R., 2004, *MNRAS*, **351**, 1379
- Schruba A., et al., 2012, *AJ*, **143**, 138
- Shectman S., Johns M., 2010, in *Ground-based and Airborne Telescopes III*. p. 77331Y, doi:10.1117/12.857852
- Sibthorpe B., Helmich F., Roelfsema P., Kaneda H., Shibai H., 2015, in *EAS Publications Series*. pp 411–417, doi:10.1051/eas/1575083
- Simón-Díaz S., Stasińska G., 2011, *A&A*, **526**, A48
- Sofia U. J., Jenkins E. B., 1998, *ApJ*, **499**, 951
- Somerville R. S., Davé R., 2015, *ARA&A*, **53**, 51
- Spergel D., et al., 2013, preprint, ([arXiv:1305.5425](https://arxiv.org/abs/1305.5425))
- Spinoglio L., Pereira-Santaella M., Dasyra K. M., Calzoletti L., Malkan M. A., Tommasin S., Busquet G., 2015, *ApJ*, **799**, 21
- Spinoglio L., et al., 2017, PASA, this issue
- Spitzer Jr. L., 1948, *ApJ*, **107**, 6
- Spoon H. W. W., et al., 2006, *ApJ*, **638**, 759
- Stasińska G., Szczerba R., 1999, *A&A*, **352**, 297
- Swinyard B., et al., 2009, *Experimental Astronomy*, **23**, 193
- Tremonti C. A., et al., 2004, *ApJ*, **613**, 898
- Tsamis Y. G., Péquignot D., 2005, *MNRAS*, **364**, 687
- Tsamis Y. G., Barlow M. J., Liu X.-W., Danziger I. J., Storey P. J., 2003, *MNRAS*, **338**, 687
- Verma A., Lutz D., Sturm E., Sternberg A., Genzel R., Vacca W., 2003, *A&A*, **403**, 829
- Vermeij R., van der Hulst J. M., 2002, *A&A*, **391**, 1081
- Verner D. A., Ferland G. J., Korista K. T., Yakovlev D. G., 1996, *ApJ*, **465**, 487
- Vidal T. H. G., Loison J.-C., Jaziri A. Y., Ruaud M., Gratier P., Wakelam V., 2017, *MNRAS*, **469**, 435
- Vincenzo F., Belfiore F., Maiolino R., Matteucci F., Ventura P., 2016, *MNRAS*, **458**, 3466
- Wootten A., Thompson A. R., 2009, *IEEE Proceedings*, **97**, 1463
- Wright E. L., et al., 2010, *AJ*, **140**, 1868
- Xie Y., Li A., Hao L., 2017, *ApJS*, **228**, 6
- Zhukovska S., Dobbs C., Jenkins E. B., Klessen R. S., 2016, *ApJ*, **831**, 147
- van Hoof P. A. M., Weingartner J. C., Martin P. G., Volk K., Ferland G. J., 2001, in Ferland G., Savin D. W., eds, *Astronomical Society of the Pacific Conference Series Vol. 247, Spectroscopic Challenges of Photoionized Plasmas*. p. 363 ([arXiv:astro-ph/0107183](https://arxiv.org/abs/astro-ph/0107183))
- van Hoof P. A. M., et al., 2013, *A&A*, **560**, A7
- van Zee L., Salzer J. J., Haynes M. P., 1998, *ApJ*, **497**, L1
- van der Tak F., et al., 2017, PASA, submitted as part of this issue